Electron Dynamics in Nanocrystalline ZnO and TiO_2 Films Probed by Potential Step Chronoamperometry and Transient Absorption Spectroscopy

Richard L. Willis,[†] Carol Olson,[‡] Brian O'Regan,[§] Thierry Lutz,[†] Jenny Nelson,[‡] and James R. Durrant*[,†]

Centre for Electronic Materials and Devices, Departments of Chemistry and Physics, Imperial College, London SW7 2AY, U.K., and Energy Center Netherlands, PV Cells and Modules, P.O. Box 1, NL 1755 ZG Petten, Netherlands

Received: January 24, 2002; In Final Form: May 16, 2002

Potential step chronoamperometry is employed to compare the capacitances of nanocrystalline ZnO and TiO_2 electrodes. These capacitance data are complemented by transient optical absorption studies of charge recombination following adsorption of molecular sensitizer dyes to these metal oxide electrodes. Both measurements are conducted as a function of electrochemical bias applied to the metal oxide film in a three-electrode photoelectrochemical cell. For both metal oxides, a power law dependence was observed between the half times for charge recombination ($t_{50\%}$) and the metal oxide electron density n determined from integration of the capacitance data, $t_{50\%} \propto n^{-1/\alpha}$, where $\alpha = 0.27$ and 0.30 ± 0.05 for ZnO and TiO_2, respectively. A numerical model for the recombination dynamics based upon a random walk of electrons between localized sub-bandgap states is found to be in good agreement with experimental observations for both metal oxides. At negative applied potentials, the film capacitance, and therefore electron density, is observed to increase more rapidly with increasingly negative applied potential for the ZnO film compared to the TiO_2 film. This observation is quantitatively correlated with a more rapid acceleration of the recombination dynamics observed for dye sensitized ZnO films under negative biases. It is suggested that the faster recombination dynamics observed under negative bias may be the origin of the lower open circuit voltages reported previously for dye sensitized photoelectrochemical cells employing ZnO electrodes relative to comparable devices employing TiO_2.

Introduction

High surface area, optically transparent electrodes may be fabricated by the deposition of porous, nanocrystalline metal oxide films on conducting glass substrates. Such films are attracting widespread interest in fields such as photocatalysis, electrochromic devices, and photovoltaic cells.[1−4] They are typically fabricated from 5 to 100 nm sized metal oxide nanocrystals, sintered together to yield a continuous, porous structure. Functional applications of these films generally rely upon electrochemically or photochemically induced electron transport within the film and interfacial electron transfer events at the film surfaces. The dynamics of electron transfer and transport within such films are therefore critical to functional applications, and are in turn strongly influenced by the film morphology.

The porous, nanocrystalline structure of these films raises basic scientific questions concerning their electronic and electrochemical characteristics. First, the small size of the nanoparticles results in a very high surface area-to-volume ratio. This means that electronic properties are strongly influenced by surface related defects and adsorbed species. Second, the nanoparticle diameter is much smaller than the width of the space charge region which would be developed, for a weakly doped material, in the bulk semiconductor at the interface with an electrolyte. Since the pores between nanocrystals are filled with electrolyte, this means that nanocrystalline electrodes cannot support macroscopic electric fields, in contrast to nonporous metal oxide electrodes. Electron transport in electrolyte supported nanocrystalline electrodes is therefore considered to be driven by concentration gradients (diffusive transport) rather than electric field (drift transport).[5,6]

Attention to date has focused largely on nanocrystalline TiO_2 electrodes. Such electrodes are of interest for various functional applications and in particular for dye sensitized solar cells, which have achieved solar to electrical energy conversion efficiencies of up to 10.4%.[4] However, several recent studies have addressed the possibility of using alternative metal oxides, and in particular, nanocrystalline ZnO, in dye sensitized photovoltaic cells.[8−14] ZnO is an attractive material for such devices as it is amenable to a range of fabrication procedures such as sol gel processes,[8] chemical bath deposition,[15,16] and electrodeposition[17] which allows greater optimization of film morphology than is possible for TiO_2. ZnO furthermore has the advantage of higher electronic conductivity than TiO_2.[12] Dye sensitized photovoltaic cells employing ZnO films have recently been reported with a solar to electrical energy conversion efficiency of 5%.[14]

In the case of nanocrystalline TiO_2, electron transport is strongly influenced by trapping,[18−23] resulting in remarkably slow electron transit times across the film.[24−26] Electron traps are usually assigned to Ti^{3+} sites and are believed to result from intrinsic defects as well as surface related and intercalated species.[24]

* Corresponding author. Fax: 44 (0)20 7594 5801. E-mail: j.durrant@ic.ac.uk.
[†] Centre for Electronic Materials and Devices, Department of Chemistry.
[‡] Centre for Electronic Materials and Devices, Department of Physics.
[§] Energy Center Netherlands.

10.1021/jp020231n CCC: $22.00
Published on Web 07/16/2002

We have recently demonstrated that transient optical studies of charge recombination dynamics can be used to probe electron trapping and transport within dye sensitized nanocrystalline TiO_2 films.[21,22,27,28] Such measurements are based upon determination of the kinetics of the charge recombination reaction:

$$dye^+ + e^-_{MO} \rightarrow dye \quad (1)$$

between photogenerated dye cations (dye^+) adsorbed to the film surface and electrons within the metal oxide (e^-_{MO}), as a function of electrical potential applied to the film. We have observed a strong inverse correlation between the electron density n in the nanocrystalline TiO_2 film and the half-time $t_{50\%}$ for charge recombination of the form

$$t_{50\%} \propto n^{-1/\alpha} \quad (2)$$

where α has a value in the range 0.25−0.5, depending upon the electrolyte used.[22] This behavior is consistent with the recombination process being limited by the diffusion of electrons within an energetic distribution of trap sites in the nanocrystalline TiO_2 film. We have successfully simulated the behavior using a numerical model of charge transport[21] on the basis of the continuous time random walk model of Scher and Montroll.[29] The conclusion of this work is that charge trapping and de-trapping within the TiO_2 film is the rate-limiting step in the recombination reaction 1. It follows that the density, energetics, and physical location of trap sites within the metal oxide film are critical to device function.

While there have been extensive studies of both electron dynamics and trap states in nanocrystalline TiO_2 films, comparable studies of nanocrystalline ZnO films have been limited to date. Existing studies are inconclusive, in particular on the role of electron trap states in nanocrystalline ZnO and their effect on electron dynamics. The importance of trap states in ZnO was identified by Hoyer and Weller[10] who observed potential dependent photocurrent kinetics in dye sensitized colloidal ZnO, which could be attributed to the filling of deep electron traps. Van Dijken et al. concluded from photoluminescence studies that deep hole traps, probably introduced by oxygen deficiency, dominate luminescence but that electron traps are relatively unimportant or shallow.[30] De Jongh et al.[13] used intensity modulated photocurrent and photovoltage spectroscopy to study electron transport in illuminated ZnO electrodes, and concluded that interparticle transport is rapid and that the density of electron trap states is low relative to TiO_2. However, Bauer et al.[31] concluded from transient absorption studies that the kinetics of electron transfer to the dye cation are identical in nanocrystalline ZnO and TiO_2 films.

One difficulty in the study of trap states in ZnO, relative to TiO_2, is the absence of an optical signature of trap filling. Studies of TiO_2 have exploited the blue-black coloration of the films associated with Ti^{3+} state formation[40] to monitor the filling of traps. No such strong coloration is observed upon the reduction of ZnO films (until the onset of ZnO reduction to zinc metal), and studies of trap occupancy in such films are therefore limited to indirect optical (e.g., Burstein shift[9]) and electrochemical[10] techniques.

The aim of this paper is to clarify the role of electron traps in nanocrystalline ZnO and their influence on electron transfer kinetics. We employ electrochemical and spectroelectrochemical techniques to monitor trap filling in structurally analogous nanocrystalline TiO_2 and ZnO films. We correlate these trap filling studies with transient spectroscopic measurements of interfacial charge recombination dynamics in these films. We conclude that in ZnO, as in TiO_2, charge recombination appears to be controlled by trap-limited electron diffusion within the metal oxide network.

Materials and Methods

Film Fabrication. All chemicals used in these syntheses were obtained from Sigma-Aldrich or their subsidiaries. Nanocrystalline TiO_2 films were prepared from a sol−gel colloidal paste containing 12.5%/wt ~15 nm TiO_2 particles and 6.2%/wt Carbowax 20 000 [Fluka], essentially following the methodology published by Barbe et al.[32] and by Topoglodis.[33] For preparation of the colloidal paste, 25 mL of titanium isopropoxide was injected into 5.5 g of glacial acetic acid under argon and stirred for 10 min. The mixture was then injected into 120 mL of rapidly stirred 0.1 M nitric acid in a conical flask. The flask was left uncovered and heated at 80 °C for 8 h. After cooling, the solution was filtered using a 0.45 μm syringe filter, diluted to 5%/wt TiO_2 by the addition of H_2O, and then autoclaved at 220 °C for 12 h. The colloids were re-dispersed with a 60 s full power burst from a LDU Soniprobe sonic horn, and then the solution was concentrated to 12.5% on a rotary evaporator using a membrane vacuum pump at a temperature of 40 °C. 6.2%/wt Carbowax 20 000 was added, and the resulting paste was stirred slowly overnight to ensure homogeneity and that no air bubbles were trapped in it. Films 8 μm thick were deposited by doctor blading the paste between double thickness strips of Scotch Magic Tape placed along the edges of TEC-15 F:SnO_2 conducting glass microscope slides. The films were left to dry in air until they were transparent then sintered at 450 °C for 20 min in an ashing furnace. The titania films were highly transparent with a transmission of >80% (effective OD < 0.1) for wavelengths >450 nm.

Zinc oxide particles were prepared by Hilgendorf[34] with an additional step to increase the average particle size and remove the side product tetramethylammonium acetete from the paste before film fabrication. The colloids were formed by first adding 37 g of dry zinc acetate (prepared fresh by mixing $ZnAc \cdot 2H_2O$ with acetic anhydride, in argon atmosphere) to 90 mL of 25% tetramethylammonium hydroxide (TMA-OH) in methanol and stirring rapidly under argon at 40 °C for 2 h. After drying in a rotary evaporator the sample was ground (in a glovebox) and stored under dry nitrogen until required. Five grams of the resulting powder were added to an equal mass of 99.9% ethanol and heated at reflux for 1 h. This changed the initially clear solution to a milky white as the colloids increased in size. The colloids were allowed to settle out of the solution and were then washed with dry ethanol by several decantation /readdition steps to remove the TMA-acetate. After a final decantation, the colloids (around 15% /w in ethanol) were mixed with small aliquots of 7% solution of ethylcellulose in ethanol, followed by stirring, until the suspension reached a slightly viscous state suitable for "doctor blading". Films (4 μm thick) were then produced by doctor blading (as above, using one thickness of tape) and then sintered at 400 °C for 20 min. The zinc oxide films were again highly transparent with a tranmission of >60% (effective o.d. <0.2) for wavelengths >450 nm.

Microscopy. Microscopy was carried out on each film sample using a Philips XL-30 Field Emission Scanning Electron Microscope to establish film thickness and estimate the average particle size.

Spectroelectrochemical and Electrochemical Characterization. Electrochemical studies were conducted in three-electrode photoelectrochemical cells employing MeCN based nonredox active electrolytes containing 0.1M tetrabutylammo-

nium perchlorate (TBAP) and 0.1 M lithium perchlorate unless otherwise stated. To minimize the water present in the electrolyte, the MeCN was distilled over CaH_2 under a nitrogen atmosphere just prior to use, the TBAP was heated at 100 °C for 12 h, and the lithium perchlorate was heated at 150 °C under vacuum for 12 h. The water content of the resulting electrolytes was determined using a Metrohm 737 Coulometer. All electrolytes used had values of 200−600 ppm H_2O.

Prior to all electrochemical experiments, the 1 cm^2 section of ZnO or TiO_2 film on conducting glass to be examined was heated to either 400 °C or 450 °C, respectively, for 10 min to remove adsorbed moisture and organics. The film was then held in a platinum clip and used as the working electrode in a photoelectrochemical cell. The counter electrode was fine platinum mesh and an Ag/AgCl reference electrode was used with an AutoLab PGStat 12 potentiostat to provide potential control in the experiment. Argon was bubbled slowly next to the working electrode between readings to maintain an anaerobic atmosphere and to provide efficient mixing of the electrolyte throughout the experiment.

For chronoamperometric studies, the cell was left at +200mV vs Ag/AgCl ref. for 10 min to allow equilibrium to be reached. A bias step of −25mV was then applied, the current transient recorded (∼50k samples /s) and integrated as detailed below. The same procedure was carried out at 100 mV intervals, with the sample held at the new voltage for 5 min prior to the 25 mV step to allow stabilization of the dark current. In the case of the ZnO electrodes the applied potential was limited to ≥ −625 mV in order to avoid reduction of the electrode to Zn metal, observed as an irreversible darkening of the electrode at more negative potentials.

For spectroelectrochemical studies, the photoelectrochemical cell was placed in the sample compartment of a Shimadzu 1601 UV−vis spectrometer. The film absorption spectrum (uncorrected for sample scatter) was recorded between 400 and 900 nm. Voltage increments of 100mV were applied, starting at +200 mV vs Ag/AgCl and finishing at −1000 mV with the spectrum collected 5 min after each voltage increment was applied.

Each electrochemical and spectroelectrochemical experiment was repeated on at least two nominally identical film samples. The experimental results were found to show a good level of reproducibility (within ±50 mV on curve position along the *x*-axis). For TiO_2 films, chronoamperometric data were collected for films with and without adsorbed sensitizer dye for potentials up to the steady-state dye reduction potential; no difference was observed between these data sets.

Transient Spectroscopy. Transient absorption studies of dye sensitized nanocrystalline films were conducted as detailed previously.[28] Nanocrystalline Zinc oxide and TiO_2 films were sensitized with the sensitizer dye Ru(HP-terpy)(Me_2-bpy)-(NCS)[43] by immersion of preheated films overnight. This dye was dissolved in 70:30 ethanol:dimethyl sulfoxide (DMSO) solution at 10^{-4} M concentration. Control experiments employed TiO_2 films sensitized as previously with $Ru(dcbpy)_2(NCS)_2$.[27]

The optical density of the films was between 0.3 and 0.6 at a pump wavelength of 520 nm. The Ru(HP-terpy)(Me_2-bpy)-(NCS) sensitizer dye, which binds to the TiO_2 surface through a phosphonate group, was selected to avoid problems of instability of the ZnO oxide electrode which have been reported previously when using dyes incorporating carboxylate type binding groups.[35] The dye sensitized films were placed into the photoelectrochemical cell as detailed above. For determination of the transient absorption data, samples were excited at 520 nm with pulses from a nitrogen laser pumped dye laser (<1ns pulse duration, 0.9 Hz). The resulting photoinduced change in optical density was monitored employing a 100 W tungsten lamp light beam with 20 nm bandwidth monchromators before and after the sample, home-built detection electronics and digitized on a TDS-220 Tektronics DSO. Typically data from 16 laser pulses were averaged for each time scale for the trace shown.

Particular care was taken to minimize desorption/degradation of the sensitizer dye induced by negative applied potentials. Data were collected at zero or positive applied potentials before and after all experiments. Comparison of these data indicated that in all cases any such deterioration reduced the transient signal by no more than 10%, and caused no detectable change in the charge recombination dynamics.

Modeling. Charge recombination kinetics were simulated using the model described in refs 21 and 22. This is a Monte Carlo simulation where electrons diffuse on a lattice by moving to nearest neighbor sites. Initially *n* electrons and a single dye cation are implanted at random on to a cubic lattice embedded in a spherical shell. A fraction of the sites are trap sites and have energies distributed according to an exponential density of states function,

$$g(E) = \frac{\alpha N_t}{kT}\exp\left(\frac{\alpha E}{kT}\right) \quad (3)$$

where N_t is the density of trap states per unit volume, E the trap energy relative to the conduction band edge ($E < 0$), T is the temperature, k is Boltzmann's constant, and α is a constant between 0 and 1. The remainder of sites are conduction band sites with $E = 0$. The time for each electron to move is determined by the release time from the site currently occupied, as detailed in ref 21. At each step, the electron with the shortest waiting time is moved to a nearest neighbor site at random, and the times of all others are advanced by that waiting time. Multiple occupancy is prevented in order that Fermi Dirac statistics be obeyed. Recombination occurs whenever an electron moves on to the site occupied by the dye cation.

The lattice dimensions were chosen as in ref 22. The choice of α, for each material system, and *n*, for each bias, is explained below. Simulations are repeated 5000 times for each value of *n* to obtain a graph of the cation survival probability as a function of time. This is to be compared with the transient absorption decay curve, normalized to its initial amplitude. The time scale of the simulation is chosen to obtain the best fit between the set of modeled and measured curves for each material system.

Results

Structural Characterization. Scanning electron micrograph images (Figure 1) were obtained from the nanocrystalline TiO_2 (a) and ZnO (b) films. It is apparent that both films exhibit mesoporous structures typical of films employed in dye sensitized photoelectrochemical solar cells, although the ZnO film appears somewhat more homogeneous than the TiO_2 film. The particle sizes estimated from such images were 10−15 nm and 15−20 nm for the TiO_2 and ZnO films, respectively. The difference in the particle size between the films (and the associated small morphological changes) is the cause of the slightly increased optical density of the zinc oxide films mentioned above. The pore volume fractions for the films, determined from their mean densities by weighing a known volume of film, were determined to be 50 ± 5% solids for both metal oxides.

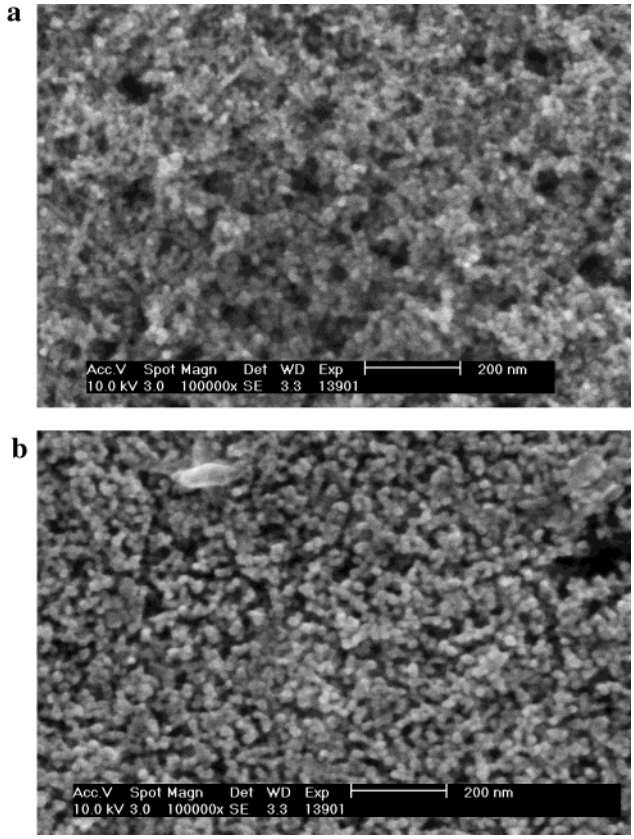

Figure 1. Scanning electron micrograph images of (a) nanocrystalline TiO_2 and (b) nanocrystalline ZnO films at high resolution (100k × magnification).

Electrochemical Studies of Electron Occupancy. Cyclic voltammetry has been used by several groups to probe trap filling in nanocrystalline metal oxide films. Typical cyclic voltammograms for the TiO_2 and ZnO are shown in Figure 2. Both voltammograms show the hysteretic shape characteristic of electron accumulation/discharge in the nanocrystalline film, superimposed upon faradic currents into the electrolyte. We note, however, that, particularly for the case of the TiO_2 films in the nonaqueous solvents used in these experiment, the voltammograms obtained were strongly dependent upon the scan rate employed, complicating interpretation of such voltammograms in terms of the film capacitance. As we demonstrate below this behavior derives from multiple time scales for electron flow into the nanocrystalline film.

Chronoamperometry has previously been shown to be an alternative probe of electron occupancy in nanocrystalline metal oxide films.[10,36] In this technique, a potential step is applied to the metal oxide/electrolyte junction, and the resulting transient current recorded. Figure 3a,b show typical chronoamperometric current transients recorded for TiO_2 and ZnO films in the photoelectrochemical cell. All transients exhibit an initial "fast" phase, which is complete within 1 s for all but the most negative voltages applied. In the case of the TiO_2 electrodes, a second, slower phase is also observed which becomes more prominent with increasing negative potential. This slow phase was not observed for the ZnO films. In all cases there is, in addition, a change in the dark current, due to a change in the steady-state resistance of the junction as applied bias is changed.

The fast phase observed for both films is attributed, as previously,[10] to capacitative charging of the film (and substrate) and can be modeled by a single-exponential decay, as expected for standard RC behavior.[10] This phase is therefore assigned to

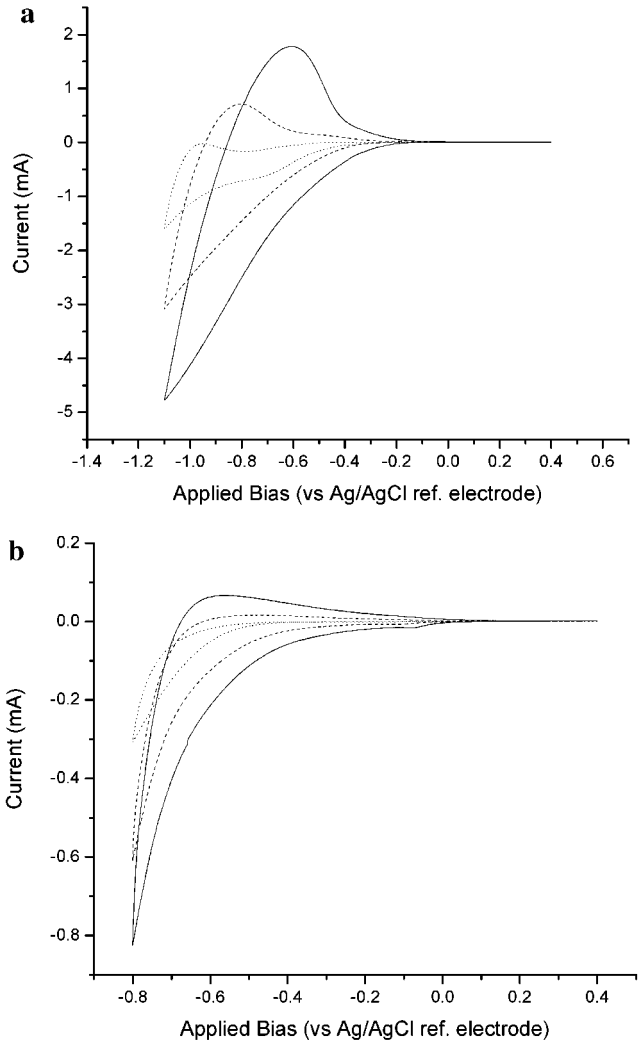

Figure 2. Cyclic voltammograms of 8 μm TiO_2 (a) and 4 μm ZnO (b) films collected in three-electrode photoelectrochemical cell at scan rates of 0.1 V/s (solid line) 0.05 V/s (dashed line) 0.007 V/s (dotted line). The experiment employed an anhydrous acetonitrile electrolyte containing 0.1M tetrabutylammonium perchlorate and 0.1M lithium perchlorate. All voltages are shown relative to an Ag/AgCl reference electrode.

capacitative charging of the film, and is analyzed in detail in this paper. This focus is based on transient absorption studies presented elsewhere[7] which demonstrate that any charging processes associated with the slow phase do not influence the charge recombination dynamics. It is further supported by the good correlation observed between the electron occupancy due to this fast phase with the experimentally observed charge recombination dynamics, discussed below. We note that biphasic chronoamperometry kinetics have recently been reported for nanocrystalline TiO_2 films in aqueous electrodes; in this case, however, the authors focused primarily on determining the slower phase of chronoamperometry data.[36] Further discussion of the slow phase observed for the TiO_2 films will be presented elsewhere.[7]

Film capacitances obtained as a function of applied bias by numerical integration over time of the fast phase of the chronoamperometric data shown in Figure 3, are presented in Figure 4a. Control experiments on conducting glass electrodes without a nanocrystalline film yielded only a rapid, bias independent chronoamperometric decay assigned to charging of the Helmholtz layer at the surface of the SnO_2 substrate. This capacitance (25 μF cm^{-2}) has been subtracted from the

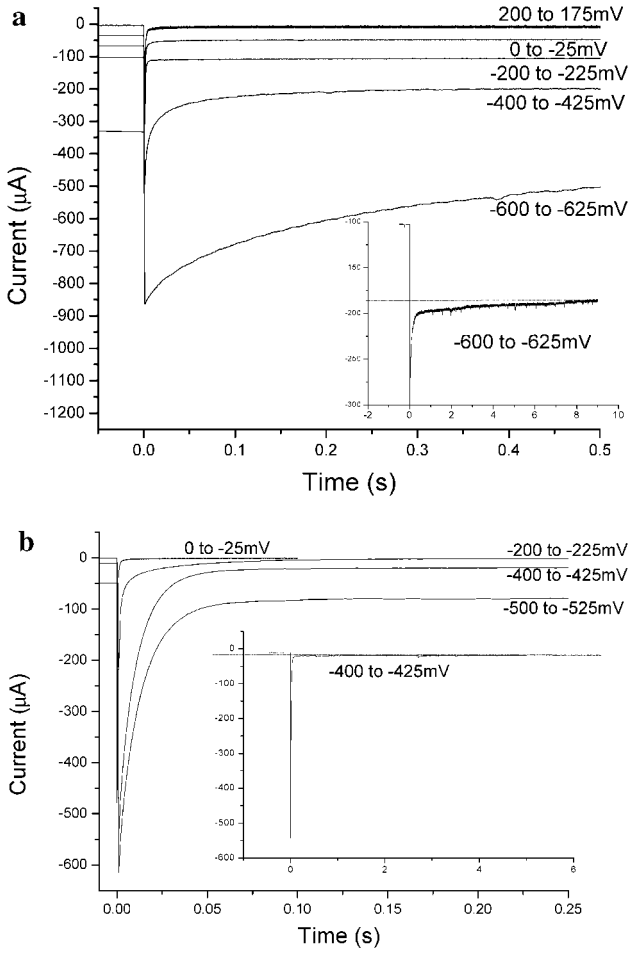

Figure 3. Chronoamperometric transients for an 8μm TiO_2 film (a) and a 4μm ZnO film (b). Experimental conditions as for Figure 2. Prior to each voltage step, the films were equilibrated at the starting potential for 5 min.

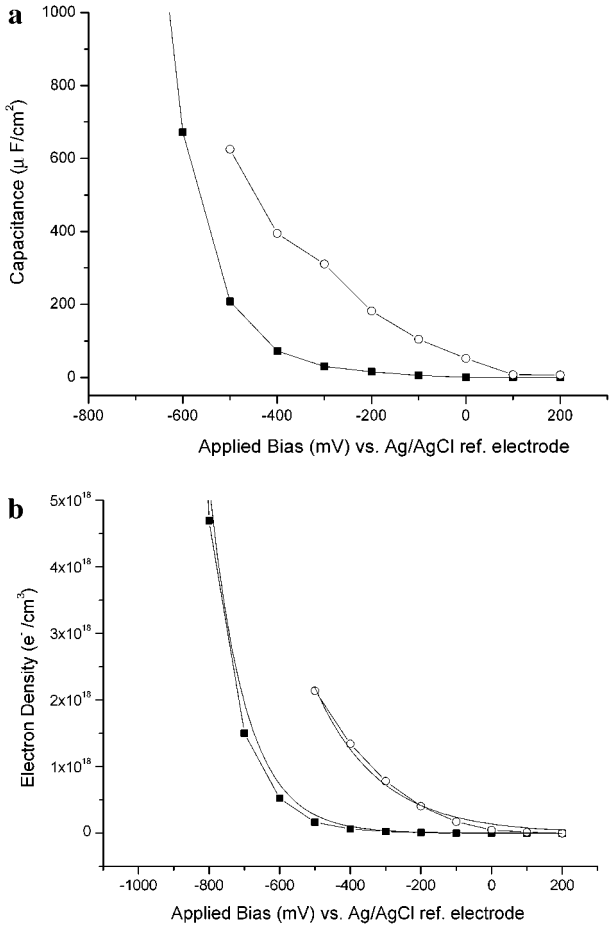

Figure 4. (a) Plot of the film capacitances obtained from the chronoamperometric data shown in Figure 3 for nanocrystalline TiO_2 (■) and ZnO (○) films. Capacitances were obtained by integration of the exponential components of the chronoamperometric traces (see text for details). (b) Plot of the electron density added to the TiO_2 (■) and ZnO (○) films over the bias ranges shown. Values obtained by integration under the curves shown in Figure 4a, scaled to give electron density per cm^3 of metal oxide. Also shown (smooth lines) are single-exponential fits to electron density data for both metal oxides.

capacitance data shown in Figure 4a. Furthermore, the film capacitance was found to be proportional to film thickness, indicating the charging process occurred throughout the film, and was not associated only with charging of the film adjacent to the SnO_2 electrode as shown in Figure 5, consistent with the conclusion of previous spectroelectrochemical experiments.[24]

The total electron density added to each film by the application of the negative bias was calculated by integration of the capacitance curves shown in Figure 4a with respect to bias from +200 mV to −1000 mV and is shown in Figure 4b. It is assumed that the accumulated electron density at +200 mV is negligible in all cases. It is apparent from Figure 4b that the electron density increases approximately exponentially with applied bias for both metal oxides: $n \propto \exp(-V/E_0)$, $E_0 = 100$ and 180 mV for TiO_2 and ZnO respectively (we note that E_0 cannot be related directly to α in eq 3 due to uncertainty over potential drops at the SnO_2/nanocrystalline metal oxide interface). It is furthermore apparent that the start of the electron accumulation is shifted by 400 ± 50 mV to more positive potentials for the ZnO films relative to the TiO_2.

The capacitance curve cannot be assigned directly to a density of states function because of uncertainties in the Fermi level shift which results from a potential step, particularly at high bias, a factor that has not always been taken into account by previous authors.[36] This is due to effects such as series resistance, Fermi level pinning at the metal oxide−electrolyte interface, and possible changes in the potential drop taken up at the substrate-metal oxide interface and the Helmholtz layer.

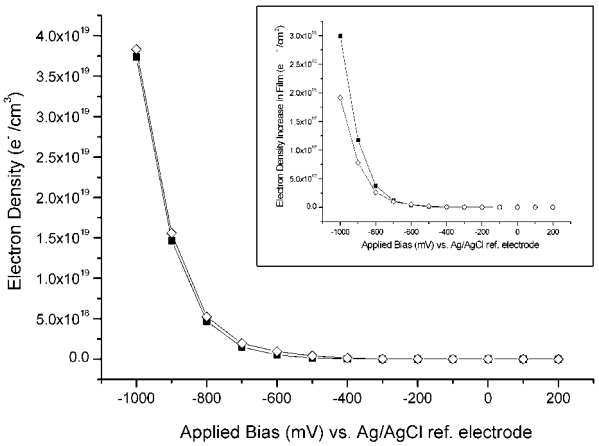

Figure 5. Plots of the integrated electron densities added to 5μm (◇) and 8μm (■) TiO_2 films as a function of the bias applied (scaled for film thickness, units e^- cm^{-3}). These electron densities were obtained from integration of chronoamperometric data and resulting capacitance data, as for Figure 4. Other experimental conditions are as for Figure 2. The inset shows the same data unscaled for film thickness (e^- cm^{-2}).

Nevertheless the fact that charge increases much more slowly with V than the Boltzmann factor, $\exp(qV/kT)$, indicates the presence of trap states in the band gap.

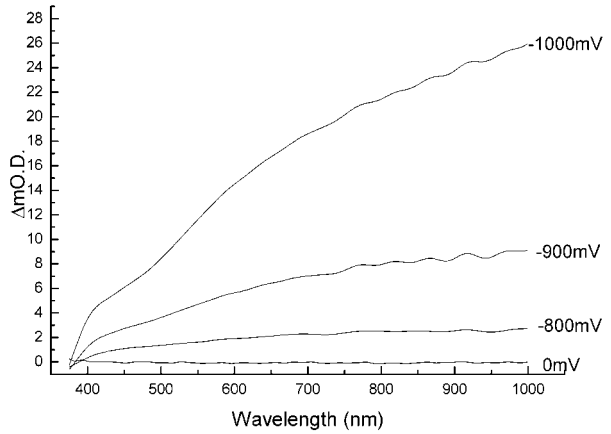

Figure 6. Spectroelectrochemical data of the absorption spectra of a 8 μm TiO_2 film as a function of applied bias. Spectra are shown relative to the spectrum obtained at +100 mV and are uncorrected for sample scatter. Other experimental conditions as for Figure 2. Spectra were collected 5 min after each bias step.

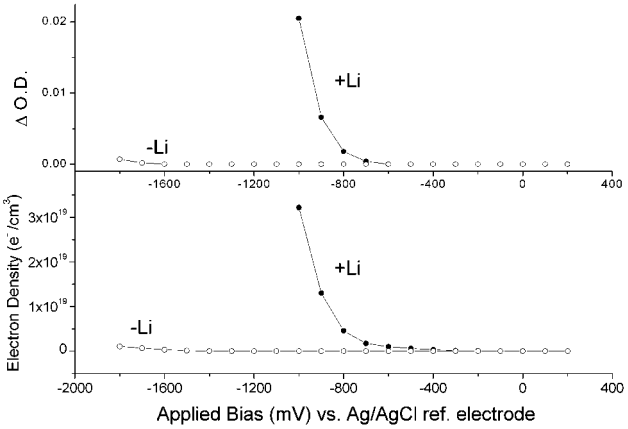

Figure 7. Spectroelectrochemical data at 800 nm (top) and electron density determined from chronoamperometric data (bottom) collected for a 8μm TiO_2 film. Conditions are as for Figure 2 with (●) or without (○) the inclusion of 0.1M lithium perchlorate in the electrolyte.

In the case of the TiO_2 films, spectroelectrochemical studies provided further confirmation that the film capacitances determined from the chronoamperometric studies were indeed associated with electron occupancy of the films. Typical spectroelectrochemical data taken at a range of voltages are shown in Figure 6. The characteristic broad absorption increase at negative applied potentials is assigned to formation of Ti^{3+} states by electrons introduced by the bias.[37−41] The change in absorption and the position of the curves with respect to bias are in agreement with those recorded by Redmond and Fitzmaurice[38] in similar conditions.

A comparison of the total charge increase in the film (Figure 4b) with the spectroelectrochemical signal monitored at 800 nm (Figure 6) is shown in Figure 7. Data are shown for the standard 0.1M TBAP/0.1M $LiClO_4$ MeCN electrolyte and also for the equivalent electrolyte with the omission of the $LiClO_4$. It has been previously shown[38] that the omission of Li^+ from such electrolytes results in a negative shift by ~1100mV of the potential dependence of the spectroelectrochemical data, attributed to the influence of such 'potential determining ions' on the energetics of Ti^{3+} formation in the TiO_2 films. It is apparent that for both electrolytes, there is a good correlation between the bias dependence of the integrated capacitance data and the spectroelectrochemical signal. This is consistent with the assignment of the capacitance data to the formation of Ti^{3+} ions in the film.

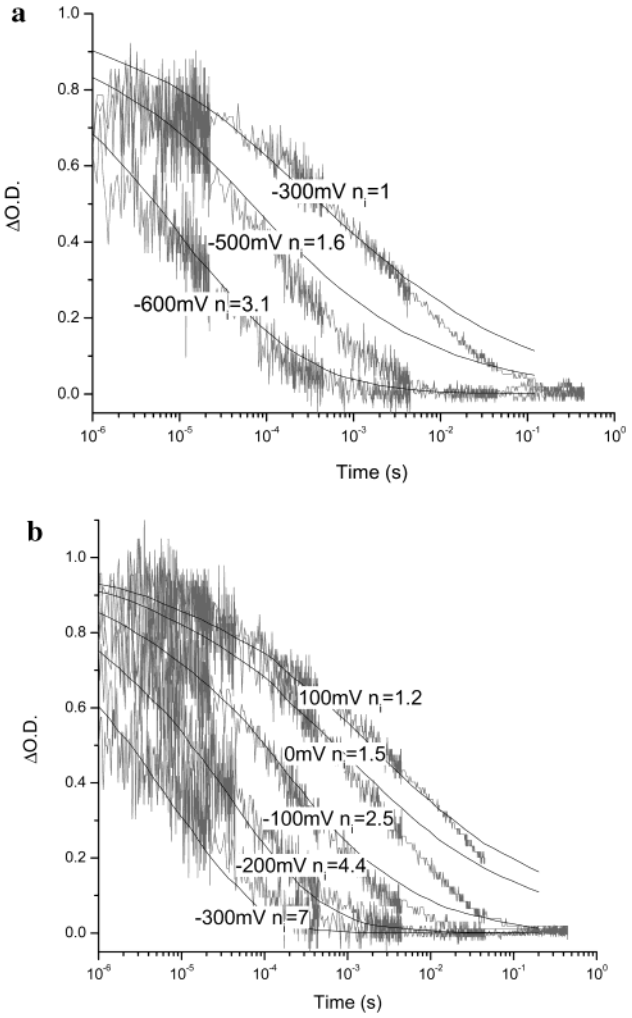

Figure 8. Transient absorption data of dye sensitized nanocrystalline TiO_2 (a) and ZnO (b) films as a function of applied bias. Data were collected at probe wavelengths of 800 and 725 nm, respectively, corresponding to the photoinduced absorption maxima of the dye cations employed. Other experimental conditions as for Figure 2. Smooth lines are simulations of these recombination data employing the CTRW model (see text details). The label on each curve gives the applied bias and the electron density (n) used to calculate the model curves. The electron densities are given as electrons per dye cation, determined from the chronoamperometric data plus the one photoinjected electron.

Correlation with Recombination Dynamics. We turn now to transient absorption studies of the charge recombination dynamics observed following absorption of sensitizer dyes to the surface of the nanocrystalline TiO_2 and ZnO films. Typical recombination dynamics as a function of potential applied to the dye sensitized metal oxide electrodes are shown in Figure 8. Transient data for ZnO films were collected for the phosophonated sensitizer dye Ru(HP-terpy)(Me_2-bpy)(NCS). For the TiO_2 electrodes, data were collected with both this dye and $Ru(dcbpy)_2(NCS)_2$, the latter being the dye widely used in the fabrication of dye sensitized photoelectrochemical solar cells. Data collected as a function of bias with these two sensitizer dyes adsorbed to TiO_2 films were indistinguishable, consistent with our previous observation that the recombination dynamics are not strongly dependent upon the identity of the sensitizer dye[42] and our conclusion that these recombination dynamics are largely controlled by the dynamics of electron transport within the metal oxide film.[22]

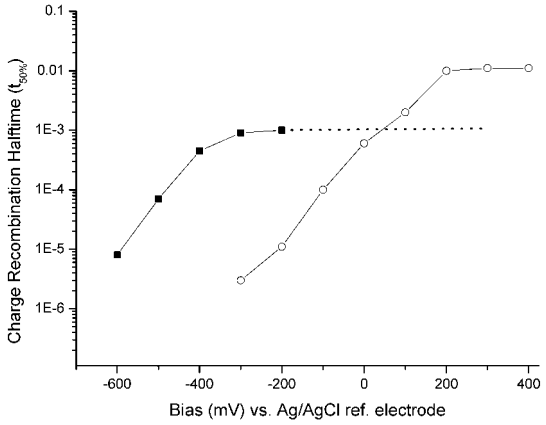

Figure 9. Half-times ($t_{50\%}$) for charge recombination determined from the absorption transients shown in Figure 8 plotted as a function of applied bias for dye sensitized nanocrystalline TiO_2 (■) and ZnO films (□). The charge recombination dynamics were independent of applied voltage for voltages > -300 mV and $+100$ mV for the TiO_2 and ZnO films, respectively.

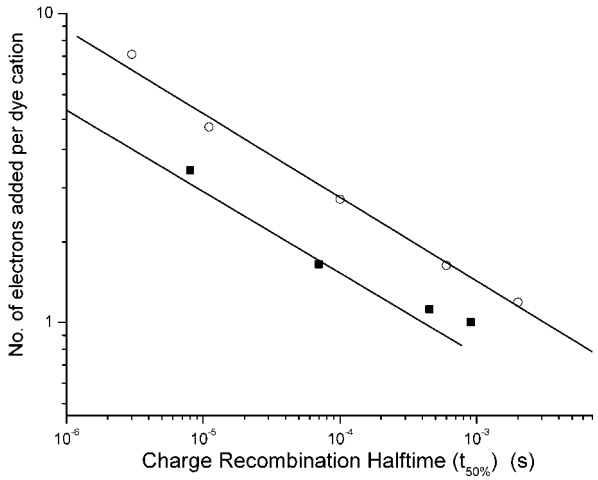

Figure 10. Log/log plots of the recombination half times determined from the transient absorption data against electron densities determined from the chronoamperometric data for the nanocrystalline TiO_2 (■) and ZnO films (○). Smooth lines are the results of model calculations employing the CTRW model (see text for details). The electron densities are given as electrons per dye cation, determined from the chronoamperometric data plus the one photoinjected electron.

The charge recombination dynamics observed for the dye sensitized TiO_2 (Figure 8a) films are similar to those we have reported previously. They exhibit both the characteristic non-exponential kinetics and strong dependence upon applied potential which we have assigned previously to recombination dynamics controlled by electron transport through an energetic distribution of trap states within the metal oxide film. It is apparent from Figure 8b that the dye sensitized ZnO films exhibit remarkably similar behavior, suggesting that recombination dynamics in these films is also limited by electron transport between trap states.

Comparison between the recombination dynamics in the dye sensitized ZnO and TiO_2 films is further illustrated in Figure 9, which plots the half-time for charge recombination ($t_{50\%}$) against the applied potential *V*. Both plots show bias independent behavior at positive potentials, with acceleration of the recombination dynamics as an increasingly negative potential is applied. As previously,[28] the bias independent region is assigned to recombination with electrons photoinjected by the laser pulse, while the acceleration at negative potentials is assigned to recombination with electrons introduced to the film by the electrical bias. It is apparent that the charge recombination dynamics at positive potentials are slowest for the ZnO electrode, but at negative potentials the recombination dynamics for ZnO accelerate rapidly, and for potentials < -100 mV vs Ag/AgCl are faster than those observed for TiO_2. A further feature is that the onset of the potential dependence of the measurements is shifted 400 ± 50 mV to more positive potentials for ZnO relative to TiO_2. This shift is in quantitative agreement with the shift in potential dependence of the electron accumulation shown in Figure 4b. We have previously demonstrated a close correlation between the electron density (*n*) and charge recombination half-time ($t_{50\%}$) for studies of dye sensitized TiO_2 films as a function of applied bias and electrolyte composition.[28] We demonstrate here that this correlation extends further to comparison of different metal oxides.

In Figure 10, we consider further the correlation between electron density and recombination half-times. In the figure the electron density, measured from the integrated capacitance data, in units of electrons per dye cation, *n*, is plotted against $t_{50\%}$ for each system. It is apparent from this figure that there is a strong correlation between *n* and $t_{50\%}$ for both the ZnO and TiO_2 electrodes. The data follow an algebraic law of the form eq 2, with exponent $\alpha = 0.27 \pm 0.05$ for ZnO and $\alpha = 0.30 \pm 0.05$ for TiO_2. In ref 22 it is shown that, if recombination is limited by electron diffusion through an exponential distribution of trap states of the form of eq 3, such a power law dependence of $t_{50\%}$ on *n* can result. The similar values of α therefore suggest a similar distribution of tail states in both ZnO and TiO_2. Note that the value of α is likely to be influenced by the electrolyte composition[22] and is not only a function of the metal oxide used. The similar dependence of $t_{50\%}$ upon *n* observed for the two electrodes is strongly indicative that, as for the TiO_2 electrodes, electron transport within the ZnO film is limited by the diffusion of electrons between an energetic distribution of trap sites. A detailed analysis of this behavior is given in the discussion below.

Figure 10 supplies the values of α and *n* needed to carry out the simulations shown in Figure 8. For each system, the value of α determined by the exponent of the data in Figure 10 is used to define $g(E)$. Then, to represent each bias, the number of electrons per dye cation determined experimentally, and plotted in Figure 10, is used for *n*. This is approximately equivalent to the number of electrons per nanoparticle. The set of decay curves for each system are fitted to the experimental data using the absolute time scale as the sole fitting parameter. The simulated decay curves are presented in Figure 8, in comparison with the data. It is clear that the model reproduces reasonably well both the bias dependence and the time dependence of the experimental curves for both metal oxides, although somewhat overestimates the experimental data at very long times.

Discussion

In this paper we have made a comparison between the behavior of TiO_2 and ZnO films. It is apparent that the ZnO films exhibit remarkably similar behavior to the TiO_2 films. An approximately exponential increase in electron density with applied bias is observed for the ZnO films, as for the TiO_2 films. A power law relationship between *n* and $t_{50\%}$ is observed for the ZnO films, as for the TiO_2 films. Moreover, as illustrated in Figure 10, numerical simulations of the recombination kinetics employing the same CTRW model used for dye sensitized TiO_2 films, are in good agreement with experimental data obtained for dye sensitized ZnO films. We conclude that, as for the

nanocrystalline TiO_2 films, electrons injected into the ZnO by external bias are functionally trapped, either by specific defect sites (e.g. oxygen defects or surface states), or by self-trapping due to lattice relaxations. Following optical excitation of dye sensitized ZnO films, charge recombination is rate limited by electron diffusion between a distribution of trap sites.

The importance of trap states in controlling the dynamics of electron transport in nanocrystalline TiO_2 is well established. We have recently shown that the model used here,[21,22,28] which is based upon electron transport between a shallow energetic distribution of trap states, is in good agreement with charge recombination dynamics in dye sensitized nanocrystalline TiO_2 films. However, the functional importance of traps in the electron transport of nanocrystalline ZnO films is less well established. Previous studies have identified the importance of hole trapping observed following band gap excitation of ZnO films,[30] or the importance of deep electron traps.[10] Deep electron traps could not explain our results since, once filled, they would remain occupied for the duration of the experiments reported here. Our own studies indicate an approximately exponential increase in the occupancy of trap states for our nanocrystalline ZnO films as a function of applied bias, indicative of a shallow exponential tail of trap states below the ZnO's conduction band edge. Such an exponential density of states has been reported in previous studies of nanocrystalline TiO_2.[21−23,44]

The bias dependence of electron occupancy and the recombination dynamics are both shifted 400 ± 50 mV to more positive potentials for ZnO relative to TiO_2 (figures 4b and 9 respectively). Previous spectroelectrochemical studies of nanocrystalline ZnO and TiO_2 films in aqueous solvents have indicated a 160 mV positive shift of flat band potential of ZnO relative to TiO_2,[9,38,39] significantly smaller than the shift we report here. This difference in the relative energetics of the two materials may derive at least in part from the electrolytes employed, and specifically our use of an acetonitrile based rather than aqueous electrolyte. We note that in aqueous solvents a Nernstian behavior of the flat band potential as a function of pH is observed (i.e.: approximately −60 mV shift per pH unit) for both metal oxides.[38,39] However, in aprotic solvents such as acetonitrile, a more complex dependence upon both effective proton activity and the concentration of other "potential determining ions" such as Li^+ is observed.[37] We furthermore emphasize that our own studies have focused upon the energetics of low energy trap states, rather than a measurement of the flat band potential, the latter corresponding effectively to the conduction band edge of the film. Our focus upon the trap states is motivated by our observation that the occupancy of these states is functionally important in determining the charge recombination dynamics in both films. We conclude that the high electron density we observe here for the ZnO films relative to the TiO_2 can most probably not be fully explained by a difference in conduction band edge between the two materials, but is indicative of a higher density of interband gap states in this metal oxide. We note that the possible presence of a significant tail of trap states below the conduction band edge of ZnO has been neglected in recent studies of the function of composite ZnO/SnO_2 dye sensitized solar cells.[45] It could explain the apparent localization of injected electrons upon ZnO even under conditions when the conduction band edge for the ZnO is thought to be above that of SnO_2.

For both metal oxides, the recombination dynamics are observed to be independent of applied voltage for voltages more positive than a threshold voltage, V_{th}, where $V_{th} = +100$ and -300 mV for ZnO and TiO_2, respectively. Comparison with the electron density data indicate that for both metal oxides this voltage independent region corresponds to biases at which the density of electron introduced by the applied bias is <1 electron per dye cation. As we have discussed previously,[28] under these conditions, charge recombination will be dominated by electrons injected by the excitation laser pulse (1 per cation), and will be independent of applied bias over this potential range ($V > V_{th}$). It is also apparent from Figures 8 and 9 that the recombination dynamics for $V > V_{th}$ are approximately 1 order of magnitude slower for the ZnO sensitized films relative to the TiO_2 films. The origin for this is unclear. Both experiments were conducted for similar densities of absorbed photons. The difference cannot be attributed to differences in the sensitizer dye employed as indistinguishable data were obtained for the two dyes absorbed to TiO_2 electrodes. The slower recombination dynamics observed for $V > V_{th}$ for the dye sensitized ZnO films may possibly arise from the photoinjected electrons being trapped in a deeper traps relative to the conduction band edge for the ZnO films compared to TiO_2 (the CTRW model requires thermal excitation to the conduction band for electron diffusion). The presence of a significant density of deeper traps in ZnO compared to TiO_2 is consistent with the 400 mV shift in the voltage dependence of the electron densities observed from our chronoamperometric data, as we discuss above.

Bauer et al. have recently reported[31] a comparison of charge recombination dynamics in dye sensitized nanocrystalline TiO_2 and ZnO thin films. They observed very similar recombination dynamics for the two films, in contrast to our own observations. However, we note that the studies of Bauer et al. were conducted without external bias control of the metal oxide fermi level and therefore without external control of the electron occupancy of the films. As we show here, the recombination dynamics in both metal oxide films are strongly dependent upon electron occupancy, and therefore applied bias. From, for example, Figure 9, it is apparent that at an applied potential of approximately 0 mV versus Ag/AgCl similar recombination dynamics are observed for the two metal oxides as reported by Bauer. However, for voltages >0 mV, recombination dynamics are fastest for the TiO_2 films, while for voltages <0 mV, recombination dynamics are fastest for the ZnO films.

Dye sensitized photoelectrochemical cells employing ZnO films generally yield lower open circuit voltages (V_{oc}) than comparable devices employing TiO_2.[14] Our own studies yielded a V_{oc} of 465 mV for a dye sensitized nanocrystalline ZnO photoelectrochemical cell, approximately 150 mV less than that observed for equivalent devices employing TiO_2 (B. O'Regan, unpublished data). The lower V_{oc} attainable for devices employing ZnO film is a significant limitation on the viability of this metal oxide for use in such devices. The results we present here provide a strong indication for the origin of this difference in V_{oc} between the two metal oxides. At a given (negative) applied potential, the ZnO film shows a higher density of electrons (Figure 4) which in turn results in faster recombination dynamics by a factor of up to 4000 (Figure 9). These faster recombination dynamics can be expected to lead to greater recombination losses for devices operating under load. Such recombination losses, both to oxidized dyes and/or oxidized redox couple in the electrolyte (i.e.: I_2/I_3^-), are thought to be the primary factor limiting the output voltage of dye sensitized solar cells.

Acknowledgment. We thank Michael Hilgendorf for supply of ZnO nanoparticles, Md. Nazeeruddin and Johnson Matthey Ltd for the supply of sensitizer dyes, Richard Monkhouse for

excellent electronics support, the EPSRC for financial support, and Saif Haque for helpful discussions.

References and Notes

(1) Mills, A.; Wang, J. S. *Z. Phys. Chem.* **1999**, *213*, 49.
(2) Kalyanasundaram, K.; Grätzel, M. *Coord. Chem. Rev.* **1998**, *177*, 347.
(3) Hagfeldt, A.; Grätzel, M. *Chem. Rev.* **1995**, *95*, 49.
(4) Hagfeldt, A.; Grätzel, M. *Acc. Chem. Res.* **2000**, *33*, 269.
(5) Rensmo, H.; Lindstrom, H.; Sodergren, S.; Solbrand, A.; Hagfeldt, A.; Lindquist, S. E. *J. Electrochem. Soc.* **1996**, *143*, 3173.
(6) Rensmo, H.; Sodergren, S.; Patthey, L; Westermark, K; Vayssieres, L.; Kohle, O.; Bruhwiler, PA.; Hagfeldt, A.; Siegbahn, H. *Chem. Phys. Lett.* **1997**, *274*, 51.
(7) Olsen, C.; Willis, R. L.; Nelson, J.; Durrant, J. D. Paper in preparation.
(8) Hoyer, P.; Eichberger, R.; Weller, H. *Ber. Bunsen-Ges. Phys. Chem.* **1993**, *97*, 630.
(9) Redmond, G.; O'Keeffe, A.; Burgess, C.; MacHale, C.; Fitzmaurice, D. *J. Phys. Chem.* **1993**, *97*, 11081.
(10) Hoyer, P.; Weller, H *J. Phys. Chem.* **1995**, *99*, 14096.
(11) Rensmo, H.; Keis, K.; Lindstrom, H.; Sodergren, S.; Solbrand, A.; Hagfeldt, A.; Lindquist, S. E.; Wang, L. N.; Muhammed, M. *J. Phys. Chem. B* **1997**, *101*, 2598.
(12) Meulenkamp, E. A. *Phys. Chem. B* **1999**, *103*, 7831.
(13) de Jongh, P. E.; Meulenkamp, E. A.; Vanmaekelbergh, D.; Kelly, J. J. *J. Phys. Chem. B* **2000**, *104*, 7686.
(14) Weis, K. Ph.D. Thesis, Uppsala, 2001.
(15) Saeed, T.; Obrien, P. *Thin Solid Films* **1995**, *271*, 35.
(16) Obrien, P.; Saeed, T.; Knowles, J *J. Mater. Chem.* **1996**, *6*, 1135.
(17) O'Regan, B.; Sklover, V.; Grätzel, M. *J. Electrochem. Soc.* **2001**, *148*, C498.
(18) Schwarzburg, K.; Willig, F. *Appl. Phys. Lett.* **1991**, *58*, 2520.
(19) Konenkamp, R.; Henninger, R.; Hoyer, P. *J. Phys. Chem.* **1993**, *97*, 7328.
(20) De Jongh, P. E.; Vanmaekelbergh, D. *Phys. Rev. Lett.* **1996**, *77*, 3427.
(21) Nelson, J. *Phys. Rev. B* **1999**, *59*, 15374.
(22) Nelson, J.; Haque, S. A.; Klug, D. R.; Durrant, J. R. *Phys. Rev. B* **2001**, *63*, 205321.
(23) van de Lagemaat, J.; Frank, A. J. *J. Phys. Chem. B* **2000**, *104*, 4292.
(24) Cao, F.; Oskam, G.; Searson, P. C.; Stipkala, J. M.; Heimer, T. A.; Farzad, F.; Meyer, G. J. *J. Phys. Chem.* **1995**, *99*, 11974.
(25) Solbrand, A.; Lindstrom, H.; Rensmo, H.; Hagfeldt, A.; Lindquist, S. E.; Sodergren, S. *J. Phys. Chem. B* **1997**, *101*, 2514.
(26) Peter, L. M.; Wijayantha, K. G. U. *Electrochim. Acta* **2000**, *45*, 4543.
(27) Haque, S. A.; Tachibana, Y.; Klug, D. R.; Durrant, J. R. *J. Phys. Chem. B* **1998**, *102*, 1745.
(28) Haque, S. A.; Tachibana, Y.; Willis, R. L.; Moser, J. E.; Grätzel, M.; Klug D. R.; Durrant, J. R. *J. Phys. Chem. B* **2000**, *104*, 538.
(29) Scher, H.; Montroll, E. W. *Phys. Rev. B* **1975**, *12*, 2455.
(30) van Dijken, A.; Meulenkamp, E. A.; Vanmaekelbergh, D.; Meijerink, A. *J. Phys. Chem. B* **2000**, *104*, 4355.
(31) Bauer, C.; Boschloo, G.; Mukhtar, E.; Hagfeldt, A. *J. Phys. Chem. B* **2001**, *105*, 5585.
(32) Barbe, C. J.; Arendse, F.; Comte, P.; Jirousek, M.; Lenzmann, F.; Shklover, V.; Grätzel, M. *J. Am. Ceram. Soc.* **1997**, *80*, 3157.
(33) Topoglidis, E.; Lutz, T.; Willis, R. L.; Barnett, C. J.; Cass, A. E. G.; Durrant, J. R. *Faraday Discuss.* **2000**, *116*, 35.
(34) Hilgendorf, M. Ph.D. Thesis, Lehrstuhls für Silicatchemie, Fakultät für Chemie und Pharmazie, Universität Würzburg, 1998.
(35) Rensmo, J. *Chem. Phys.* **1999**, 111, 2744.
(36) Wang, H. L.; He, J. J.; Boschloo, G.; Lindstrom, H.; Hagfeldt, A.; Lindquist, S. E. *J. Phys. Chem. B* **2001**, *105*, 2529.
(37) Enright, B.; Redmond, G.; Fitzmaurice, D. *J. Phys. Chem.* **1994**, *98*, 6195.
(38) Redmond, G.; Fitzmaurice, D. *J. Phys. Chem.* **1993**, *97*, 1426.
(39) Rothenberger, G.; Fitzmaurice, D.; Grätzel, M. *J. Phys. Chem.* **1992**, *96*, 5983.
(40) Howe, R. F.; Grätzel, M. *J. Phys. Chem.* **1985**, *89*, 4495.
(41) Kolle, U.; Moser, J.; Grätzel, M. *Inorg. Chem.* **1985**, *24*, 2253.
(42) Tachibana, Y.; Haque, S. A.; Mercer, I. P.; Durrant, J. R.; Klug D. R. *J. Phys. Chem. B* **2000**, *104*, 1198.
(43) Zakeeruddin, S. M.; Nazeeruddin, M. K.; Pechy, P.; Rotzinger, F. P.; Humphry-Baker, R.; Kalyanasundaram, K.; Gratzel, M.; Shklover, V.; Haibach, T. *Inorg. Chem.* **1997**, *36*, 5937.
(44) Fisher, A. C.; Peter, L. M.; Ponomarev, E. A.; Walker, A. B.; Wijayantha, K. G. U. *J. Phys. Chem. B* **2000**, *104*, 949.
(45) Tennakone, K.; Kottegoda, I. R. M.; De Silva, L. A. A.; Perera, V. P. S. *Semicond. Sci. Technol.* **1999**, *14*, 975.